

# Taking the temperature of bifacial modules: Are they warmer or cooler than monofacial modules?

Bas Van Aken & Gaby Janssen, ECN.TNO – Solar Energy, Petten, The Netherlands

## Abstract

Bifacial cells and modules collect light falling not only on the front side of the panels but also on the rear; this additional collection of light increases the total absorbed irradiance, and accordingly the generated current. One of the remaining questions is: what temperature do bifacial solar panels operate at compared with monofacial panels? The extra light absorption at the rear will heat up the modules more, but at the same time, the parasitic heating by the absorption of infrared light is reduced, because infrared light is mostly transmitted through the glass–glass panels. In this paper, different bifacial and monofacial cell and module architectures are considered for the calculation of the energy spectra for all heat loss and absorption processes and the effective heat input. The heat transfer coefficients and the heat capacities of modules with different rear panels are given. Actual module temperatures for different layouts are presented and discussed for low- and high-irradiance (diffuse/direct) conditions in the Netherlands.

bifacial modules, a clear relation between module parameters, light/heat absorption in the silicon wafer and bifacial irradiance has so far not been published.

Bifacial photovoltaic systems also utilize the light that reaches the rear side of the PV modules to generate electricity. The rear incident light either originates from diffuse or indirect light from the sky, or from reflected light from the ground (so-called *albedo light*). The combined irradiance on the PV module will consequently be greater, leading to an increase in the generated photocurrent. This brings about the question as to whether the additional incident light also generates an increase in the actual operating temperature of these bifacial solar panels, compared with the operating temperature of monofacial modules. Since an increase in operating temperature will lead to a reduction in the output voltage of a module [7,8], this would partly offset the gain due to the bifaciality.

There are three possible responses to the question whether bifacial modules are warmer or cooler than monofacial modules:

- 1. Warmer:** the module temperature rises because of the additional absorption of light on the rear side of bifacial PV panels, and consequently the output of the bifacial modules will be lower than expected from an optical analysis alone.
- 2. Cooler:** the bifacial modules are not warmer, because the transmission of light through bifacial panels is also greater than in the case of monofacial PV panels.
- 3. Neither warmer or cooler:** there is no difference in operating temperatures.

To answer this question correctly, it is necessary to analyse the full energy balance of the PV module by taking into account not only the additional light absorption and electricity generation by the rear side of the solar cells, but also the heat transfer to the environment and the heat capacity of the different modules.

First, the energy balance will be covered in detail, and all relevant optical, electrical and thermal processes will be highlighted. The differences in the absorption, generation and loss energy spectra of monofacial and bifacial solar cells will be shown.

## Introduction

That temperature plays an important role in the module power and cell efficiency is well known – hence the importance of controlling module and cell temperatures under standard test conditions (STC). For example, PV panels with silicon-based cells have a temperature coefficient of the order of  $-0.5\%_{\text{rel}}$  per °C. PV panels that are installed in the field or on a roof, however, have no temperature control; their temperature is determined by the ambient temperature, wind and irradiance conditions, but also by the thermal properties of all module materials. Extensive research has been carried out to predict or model the temperature of regular monofacial PV panels under ‘real’ conditions, either on the basis of complicated mathematical or physical models [1] or by using numerical approximations [2].

The temperature of bifacial modules is also a topic of research interest [3,4], and an important parameter in determining the (additional) energy yield of bifacial PV systems. Soria and colleagues from CEA-INES [5] showed, for a vertical facade-integrated system with a diffuse reflector on the inner wall, that with increasing front irradiance, the temperature of bifacial modules decreases relative to that of monofacial modules. Recently, Lopez-Garcia and colleagues from JRC-ISPRA [6] published an extensive work on the temperature coefficients of bifacial crystalline silicon modules, determined using solar simulators and natural sunlight; they found that the temperature coefficients were not affected by reflecting or absorbing rear covers. For

The way in which the heat input of these samples increases with additional rear irradiance is then derived from these spectra. Next, the heat output term is evaluated from experimental heating curves. Finally, outdoor data are presented for the different single-cell devices and full-size monofacial and bifacial modules, showing the influence of the rear irradiance fraction and the albedo on the different device temperatures.

### Energy balance and theory

The energy balance of an operating (bifacial) PV system is sketched in Fig. 1. The energy input is determined by the sum of the irradiance on all surfaces of the PV module, which is a combination of: 1) direct irradiance, i.e. the beam of light directly from the sun; 2) indirect irradiance from the sky; and 3) indirect irradiance from reflected (albedo) light from the ground, caused by either sun beam or sky light. For the energy balance, the optical losses due to reflection and transmission need to be subtracted from the energy input.

All the incident light that is not reflected or transmitted is, by definition, absorbed somewhere in the solar panel. The major portion is absorbed by the absorber material, in this case the Si wafer, generating electron-hole pairs that are to be collected and generate the solar electricity. Generated electricity extracted at the maximum power point is one source of energy transfer from the module. Although ~90% of incident light is absorbed in the Si wafer, only ~20% of the energy is converted to electricity. A significant part of the absorbed energy leads to conversion losses in the Si wafer, such as thermalization, entropy generation and recombination, or is parasitically absorbed [9,10] in heavily doped emitters or surface fields or in the metallization and module materials. All these conversion and parasitic absorption losses are converted to heat, as a result of which the system heats up, resulting in heat transfer to the environment. Heat transfer to the environment occurs by convection to the ambient air, enhanced by wind, and by radiation to the sky and ground. A *steady state* (constant temperature) is achieved when the heat generated in the system equals the heat transfer to the environment.

The energy balance thus consists of:

- A heat input, determined by the bifacial irradiance and many electro-optical processes in the solar panel.
- A heat transfer, determined by the heat transfer coefficient(s) and the difference in module and ambient temperatures.
- The heat capacity of the module.

In the next section, the formula describing the relation between these parameters will be introduced.

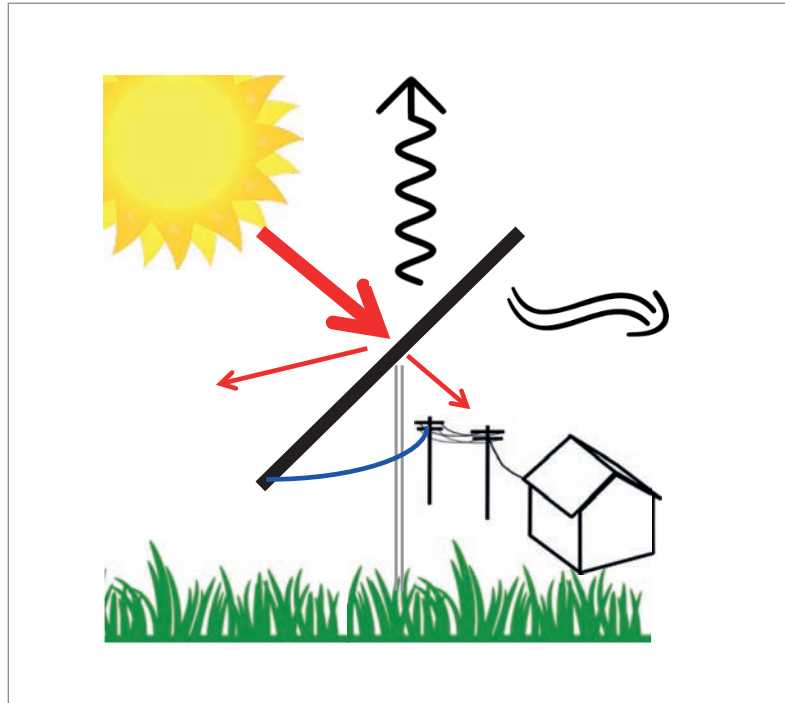


**Figure 1. Sketch of the thermal balance of a PV module. The heat input to the module is represented by the thick red arrow, corrected for reflected and transmitted light losses (indicated by thin red arrows). Energy is removed from the module by: 1) grid connection of the produced electricity (blue line); 2) radiation of heat to the sky and ground (wavy black arrow); and 3) convection of heat by the air (curved black double arrow).**

### Energy balance formula

Consider a solar device that is to be exposed to a constant irradiance. The temperature of the device is then given by an exponential heating curve as a function of time:

$$T(t) = T_{amb} + \frac{Q_{eff}}{U} \left( 1 - \exp\left(-\frac{U}{C_p} t\right) \right) \quad (1)$$

where

- $T(t)$  = module temperature as a function of time
- $T_{amb}$  = ambient temperature
- $Q_{eff}$  = the heat input
- $U$  = heat transfer coefficient
- $C_p$  = heat capacity of the panel

In this simple model, the heat transfer is assumed to be proportional to the temperature difference  $\Delta T = T(t) - T_{amb}$ , with an effective heat transfer coefficient  $U$ , which combines the effects of radiative and convective heat transfer.

Equation 1 shows that the ratio of the heat transfer coefficient  $U$  and the heat capacity  $C_p$  will determine how fast the panel heats up. The timescale of the exponential curve is characterized by a half time  $t_{1/2}$  (the time to reach one-half the steady-state value) equal to  $\ln(2) / b$  where  $b$  is given by the ratio  $U / C_p$ . The ratio  $Q_{eff} / U$  determines

**“Conversion and parasitic absorption losses are converted to heat, as a result of which the system heats up.”**

how much the temperature will increase. At steady state, the temperature  $T_{ss}$  is given by:

$$T_{ss} = T_{amb} + \frac{Q_{eff}}{U} \quad (2)$$

The heat transfer out of the device is given by:

$$Q_{out} = U \Delta T \quad (3)$$

Thus, from a heating/cooling curve under constant irradiance, the ratio  $Q_{eff} / U$  can be determined from  $T_{ss} - T_{amb}$  and the ratio  $U / C_p$  determined from the half time of the exponential fit. In the case where  $Q_{eff}$  is known, e.g. from the analysis that will be presented in the next section, the heat transfer coefficient and the heat capacity can be deduced.

### Indoor measurements

Two types of solar cell and two rear panel materials are considered in this study. The conventional, monofacial Al-BSF solar cell is compared with the bifacial n-PERT solar cell. The Al-BSF cell has a highly doped back-surface field (BSF), which is created by screen printing Al paste on the full rear surface; this paste forms an opaque Al-Si alloy. In contrast, the n-PERT solar cell's rear BSF is formed by diffusion of phosphorus [11], and this transparent BSF is contacted with an Ag metallization grid.

Both cell types were employed in monofacial single-cell mini-modules with a white backsheet (WBS) as a back reflector, and in bifacial mini-modules in a glass-glass configuration. Furthermore, two 60-cell modules were assembled with the bifacial n-PERT solar cells – one with a WBS and the other with a glass rear panel.

### Cell spectral measurements

In this section, the discussion will be about where the energy ends up when light falls on a solar device. Since the fraction of the incoming irradiance that heats the solar device needs to be determined, measurements are performed to determine what fractions of the light end up as optical losses and photovoltaic energy output, or contribute to the heating of the solar cells.

First, the optical losses. The fraction of light reflected off the solar cells or transmitted through the solar cells is measured using an integrating sphere. By convolution of these measurements with the reference AM1.5G spectrum, the absolute transmission and reflection spectra are calculated. The remaining fraction, the absorption spectrum, is calculated from the difference between the AM1.5G spectrum and the reflection and transmission spectra.

The spectral response measurement determines the spectrally resolved current contribution, in short-circuit conditions. From the spectral response measurement, the internal quantum efficiency

(IQE) is then derived. Convoluting the absorption spectrum with the IQE curve gives the sum of the electrical power and the losses due to thermalization, recombination, resistance and entropy generation, while the convolution of the absorption spectrum with the  $(1 - IQE)$  curve gives the parasitic heating. Multiplication of this spectrum by various ratios yields the electrical power spectrum, the thermalization spectrum and the remaining loss spectrum:

- *Electrical power spectrum:* multiplication by the ratio  $qV_{oc} * FF / E(\lambda)$ , where  $V_{oc}$  and  $FF$  are the short-circuit voltage and the fill factor of the cell,  $q$  is the elementary charge and  $E(\lambda)$  is the energy of a photon with wavelength  $\lambda$ .
- *Thermalization spectrum:* multiplication by the ratio  $(E(\lambda) - E_g) / E(\lambda)$ , where  $E_g$  is the band gap energy of Si.
- *Remaining loss spectrum:* multiplication by the ratio  $(E_g - qV_{oc} * FF) / E(\lambda)$ .

Fig. 2 shows these power and loss spectra for the two cell technologies. Note that the  $y$  axes – the absolute power spectral density – have different ranges in each graph in order to show more detail. In this figure, the standard monofacial Al-BSF cell, with 18.6% efficiency, is compared with an n-PERT bifacial solar cell, with 21.0% efficiency. As the Al-BSF solar cell has a lower conversion efficiency than the n-PERT solar cell, the electrical power spectrum is lower (Fig. 2(a)). Notwithstanding the difference in efficiency, there is hardly any difference ( $-0.6\%_{abs}$ ) in the sum of the thermalization, recombination and entropy generation losses between the n-PERT and the Al-BSF solar cells (Fig. 2(c)).

Larger differences are observed in the optical losses (Fig. 2(b)). The reflection is highest, but similar in magnitude, at short wavelengths, below 500nm, and at wavelengths above the band gap. In comparison, the Al-BSF cell exhibits a larger reflection than the n-PERT solar cell in the 500–900nm wavelength range. The bifacial n-PERT solar cell has a non-zero transmission (green line), especially for wavelengths around and above the bandgap of Si. The Al-BSF solar cell obviously has no transmission losses.

The parasitic absorption losses (Fig. 2(d)) see an initial peak at low UV wavelengths, and significant absorption around, and especially above, the Si bandgap. The parasitic losses are significantly higher for the Al-BSF solar cell. Of course, the Al layer at the rear of the solar cell will absorb all IR radiation that is transmitted through the Si wafer. In the n-PERT solar cell, while there is some parasitic absorption in the metallization grid and some free-carrier absorption in the highly doped regions of the emitter and the BSF, a significant portion of the IR light is also transmitted through the solar cell.

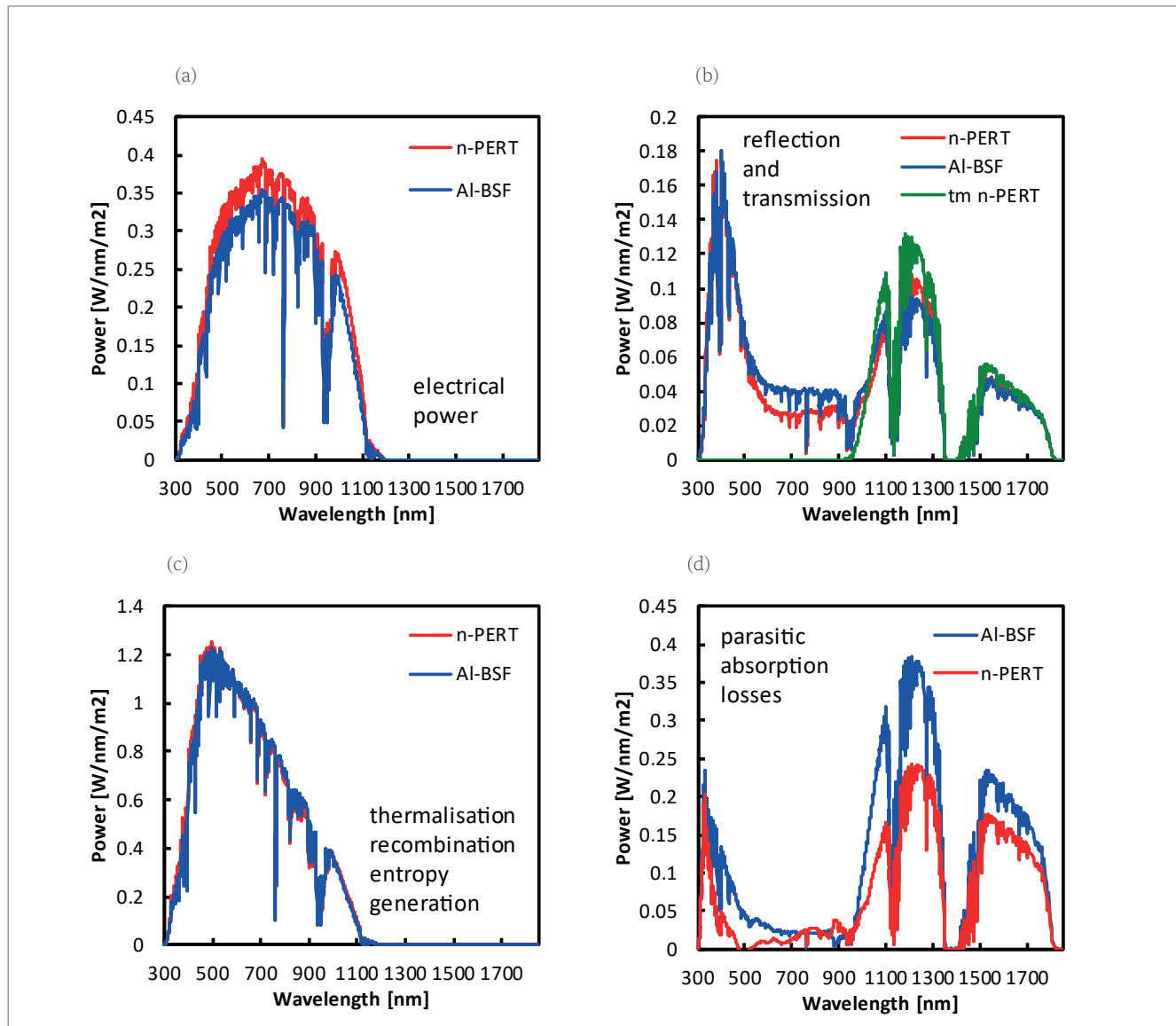


**Figure 2.** The different spectra for an Al-BSF (red) and an n-PERT (blue) solar cell: (a) electrical power; (b) optical losses, with transmission of n-PERT in green; (c) losses associated with photocurrent generation, such as thermalization, recombination and entropy generation; (d) parasitic absorption losses in metal and polymer layers.

#### Effective heat input of solar cells and modules

The effective heat input  $Q_{\text{eff}}$  of a cell or module results from the front and rear irradiation received:

$$Q_{\text{eff}} = \alpha_f G_f + \alpha_r G_r \quad (4)$$

where  $\alpha_i$  ( $i = f, r$ ) is the fraction of the incident irradiance transformed to heat,  $G_i$  ( $i = f, r$ ) is the in-plane irradiance, and the subscripts f and r stand for front and rear respectively.

In Fig. 3 the total energy of each spectrum in Fig. 2 have been integrated and their fraction plotted in the bar diagrams for both bare solar cells and cells after encapsulation in either a (monofacial) module with a WBS, or a (bifacial) module in a glass-glass configuration. Most bars show that ~55% are generation losses, ~20% is the electrical power, ~15% is due to parasitic absorption and ~5–10% are optical losses. Obvious differences with the general behaviour are observed for rear-side measurements

on WBS devices and the rear-side results for the Al-BSF solar cell in a glass-glass module. In the former samples, reflection of rear incident light by the WBS makes up the major proportion, and the remaining part, ~30%, is absorbed as heat by the backsheet. In the glass-glass module with monofacial Al-BSF solar cells, up to 80% of the light is absorbed as heat in the Al-alloy layer at the rear of the solar cell.

From the graphs in Fig. 3, the fraction  $\alpha_i$  (see Equation 4) of the incident energy that is converted to heat can be deduced by adding the conversion losses and the parasitic absorption (the red striped and solid blue regions in the graphs). Clearly, the laminates with Al-BSF cells have generally higher heating terms, specifically +3% to +8%, than in the case of laminates with n-PERT solar cells; this is because of the heat absorption of all (near-infrared) light that is transmitted through the solar cells in the Al-BSF layer. In contrast, in n-PERT solar cells, most of this light ends up as transmission losses.

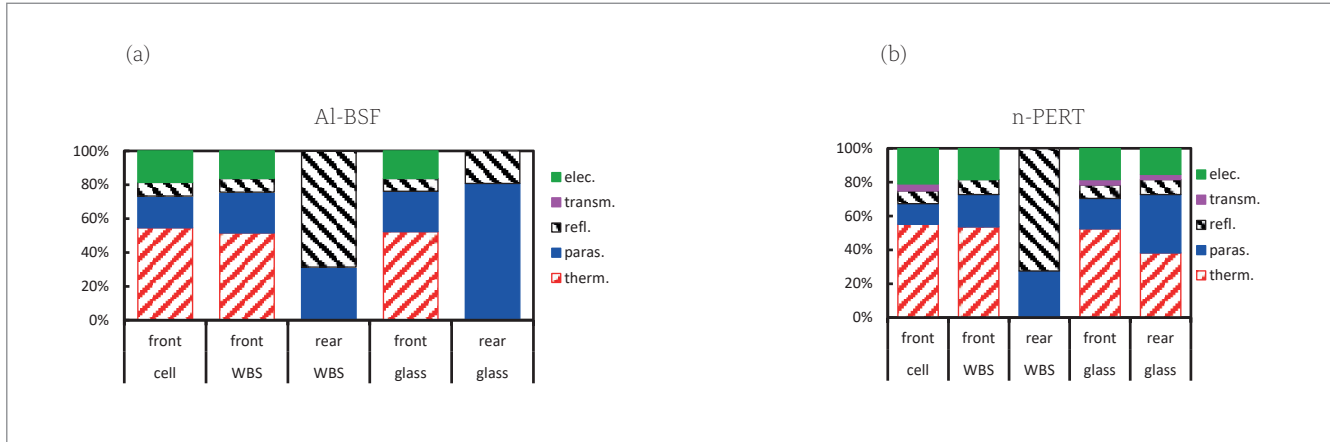


**Figure 3. Relative contributions to incident energy by various processes for (a) Al-BSF and (b) n-PERT solar cells and modules. The specific processes are electric power, transmission, reflection, parasitic heating and conversion losses ('therm.'), including thermalization, recombination and entropy generation. The five columns represent, from left to right, the front side of the solar cell, the front and rear sides of a WBS module, and the front and rear sides of a glass-glass module.**

To determine the effective heating term  $Q_{eff}$  for these solar modules, it is necessary to add the parasitic loss and the thermalization, recombination and entropy generation loss spectra and correct the result for the irradiance level. For two-sided irradiance, these spectra have also to be produced for the rear irradiance. Fig. 4 shows the effective heat generation as a function of the additional rear irradiance. Note that even monofacial cells in a glass-glass configuration, and also all modules with WBS, generate more heat when the rear irradiance increases; this heat is generated by parasitic absorption in the Al-BSF layer or in the backsheet. Fig. 4 also shows that the amount of rear irradiance determines whether the only truly bifacial module in this set (i.e. the n-PERT solar cell in a glass-glass configuration) generates more or less heat than the monofacial modules with a WBS.

The above analysis helps in determining the effective heat input for various device configuration and light conditions. This information has to be used as input data for the thermal modelling part of the energy yield modelling [12] in order to arrive at the actual operating temperature. However, the operating temperature also depends on the heat transfer coefficient, as well as on the heat capacity, when steady state has not been achieved. These parameters are discussed in the next section.

#### Module heating/cooling curves

Bifacial and monofacial modules were exposed to a constant irradiance of  $1,000\text{W/m}^2$ , with a black background environment to minimize the rear irradiance, using a steady-state solar simulator [13]. The measured module temperature as a function of the heating time for these two modules is plotted in Fig. 5, showing that the glass-glass module heats to about  $46^\circ\text{C}$ , whereas the WBS module is  $2^\circ\text{C}$  warmer in steady state; the graph also shows that the monofacial module reaches steady state significantly faster. The half times are determined from the fitted values (see Table 1): the half time for the WBS

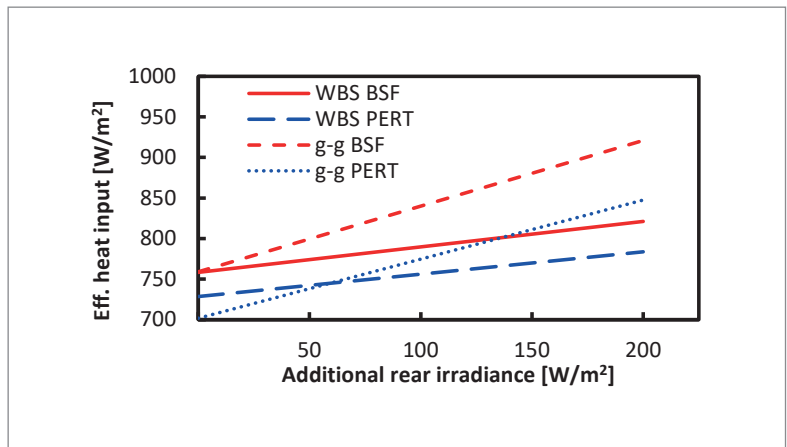


**Figure 4. Effective heating terms for the two solar cell types and the two laminate type combinations. For this calculation, a constant front irradiance of  $1,000\text{W/m}^2$  and a variable rear irradiance were assumed.**

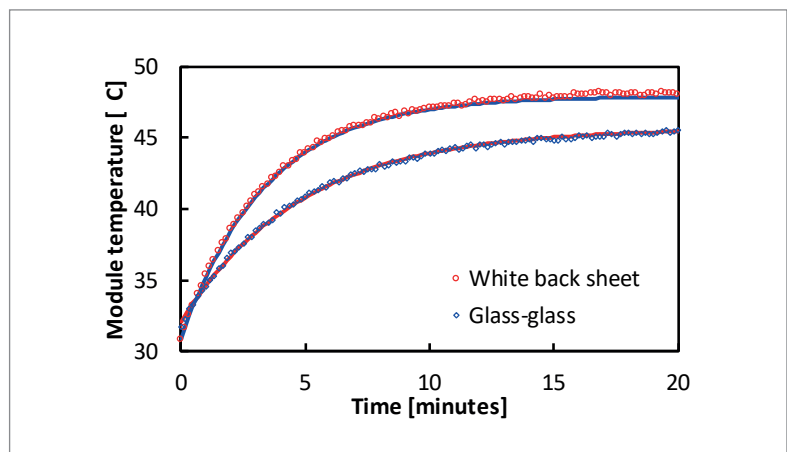


**Figure 5. Heating curve for WBS (red circles) and glass-glass (blue diamonds) modules under constant irradiance conditions. The solid lines represent exponential curves fitted to the data.**

module is only 140s, but the half time for the glass-glass module is almost 50% longer, at 200s.

The data were fitted to the exponential formula (see Equation 1). As explained in the previous section, under constant irradiance and ambient conditions,  $a$  is given by  $Q_{eff} / U$ . Likewise, the fitted parameter  $b$  determines the heating rate and is given by  $U / C_p$ .

Taking the values for  $a$  (determined from the fit)

	$T_{ss}$ [°C]	$Q_{eff}$ [W/m <sup>2</sup> ]	$U$ [W/m <sup>2</sup> /K]	$t_{1/2}$ [s]	$C_p$ [kJ/m <sup>2</sup> /K]	$C_p$ from Hoang et al. [14] [kJ/m <sup>2</sup> /K]
WBS	47.9	729	29.5	140	6.5	6.6
Glass-glass	45.7	702	31.3	200	9.9	10.1

**Table 1. Fitted and calculated values for the heating curves in Fig. 5.**

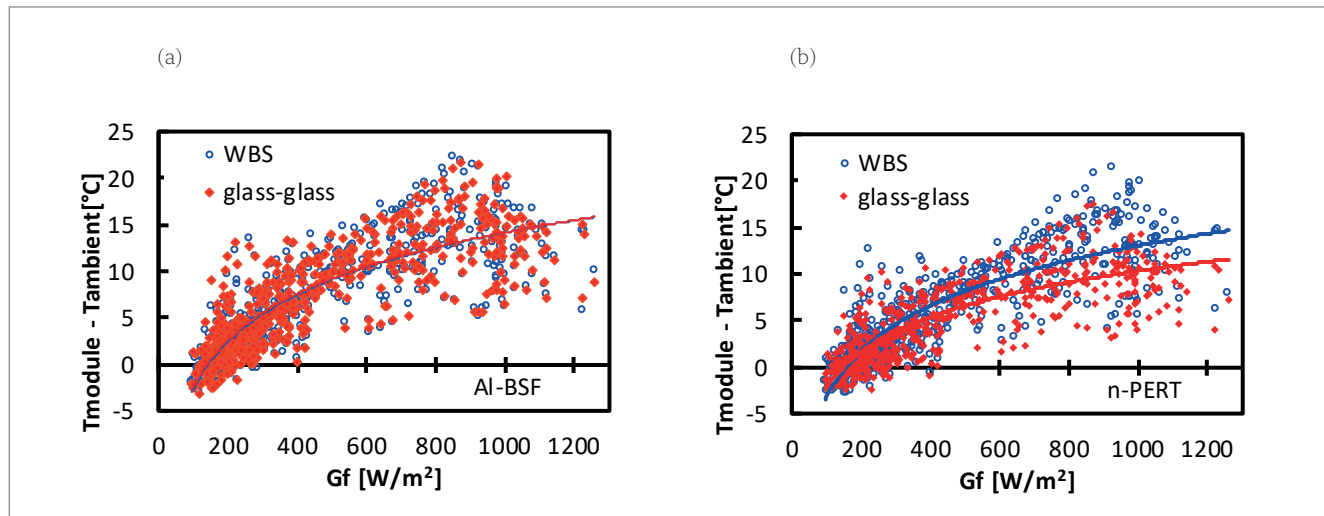


**Figure 6. Increase in module temperature relative to the ambient temperature for (a) Al-BSF and (b) n-PERT solar cells in WBS (in blue) and glass-glass (in red) module configurations. The solid lines are logarithmic fits as a visual reference.**

**“In outdoor conditions wind and relative humidity will influence the heat transfer coefficient  $U$ .**

and the calculated values for  $Q_{eff}$  (as explained by Fig. 3), the heat transfer coefficient  $U$  is calculated. From Equation 4 and the fitted value for  $b$ , the heat capacity  $C_p$  is calculated. A comparison with the heat capacity as determined from literature values for the specific heat capacities of the bill of materials is presented in Table 1. ECN.TNO's thermal model for the heating curve is validated by the good agreement between the derived experimental values for  $C_p$  and the values taken from the literature. Note that the time to reach steady state in these indoor conditions is only around 15 min.

Although in these indoor conditions the glass-glass laminate showed a 2K lower heating at  $1,000W/m^2$  irradiance, care should be taken when translating these results to outdoor conditions. Among other factors, in outdoor conditions wind and relative humidity will influence the heat transfer coefficient  $U$ , while the effective heat source term  $Q_{eff}$  will be affected by the total irradiance as well as by the ratio between front and rear irradiance, which is most relevant to outdoor conditions.

#### Outdoor measurements

In the first part of the outdoor results, single-cell laminates with the same two cell types and two rear materials as those used in the power spectrum analysis are monitored on ECN.TNO's rooftop installation [15]. In the second part, data

are presented for 60-cell modules with the same bifacial n-PERT solar cells, but with either a WBS or a glass panel as the rear material.

#### Effect of rear material choice for two different cell types

Single-cell laminates with different cell types and rear panels were installed on a rooftop at a 30-degree tilt. Data were recorded in 10-min intervals and recorded consecutively for all four samples. The irradiance was monitored to ensure constant conditions over a period of a few seconds. For each dataset, the difference between the measured module temperature with respect to the ambient temperature was determined.

Fig. 6(a) and (b) show the data for the single-cell laminates with monofacial Al-BSF solar cells and bifacial n-PERT solar cells respectively, as a function of the front irradiance for WBS or glass rear panel configurations. For clarity, a logarithmic function has been fitted to the data. The large deviations between the determined differences and the fitted curves are due to the variations in rear irradiance for a given front irradiance and the variable wind conditions. The trend in the data is clear: at a low irradiance, the modules are cooler than the ambient temperature, and with increasing irradiance, the difference increases monotonically. The Al-BSF samples show, on average, a ~14K increase, relative to the ambient temperature at  $1,000W/m^2$  front irradiance for both rear panels. The n-PERT samples with a WBS undergo a very similar increase, ~13K, but the n-PERT samples with glass as the rear panel show only a ~10K increase at  $1,000W/m^2$  front irradiance.

Although the glass–glass samples have a higher  $Q_{\text{eff}}$  (because of the rear irradiance contribution) than the WBS ones, the device temperature is not higher for the Al-BSF samples, and is in fact even lower for the n-PERT samples. Apparently, these glass–glass mini-modules have a higher heat transfer coefficient  $U$ , as was also deduced from Fig. 5. Note that the heat input term can be determined fairly accurately, but the heat transfer is much less precise, as it cannot be measured directly and depends on the module materials, geometry, humidity, wind conditions and the temperature of the air, sky and background.

**Effect of albedo**

For this investigation, a group of 60-cell bifacial and monofacial modules were measured on the outdoor rooftop set-up at ECN.TNO [15]. Data were gathered with grey concrete (red data) and with white-painted concrete (blue data) as the albedo for a period of nine months for each. Full  $I$ – $V$  curves and irradiance data are recorded every 10 min, leading to over 10,000 measurement points for each parameter, above concrete and above white paint. It is desired to determine the difference in temperature and performance of the modules for the two albedo conditions. For each measurement point, the differences in  $V_{\text{oc}}$ ,  $I_{\text{sc}}$  and module temperature are calculated. These data were summarized by averaging the rear irradiance, rear irradiance fraction and the  $\Delta V_{\text{oc}}$ ,  $\Delta I_{\text{sc}}$  and  $\Delta T$  for 20W front-irradiance bins.

Fig. 7 shows the average of rear irradiance and rear irradiance fraction, as a function of the front irradiance. Clearly, the rear irradiance increases with front irradiance for both albedo conditions. The rear irradiance fraction is 6% for grey concrete and 20% for white-painted concrete at 1,000W/m<sup>2</sup> front irradiance. In both cases, the rear irradiance fraction is higher for lower front-irradiance conditions.

The data with low front irradiance, for the location in question, combine two typical situations.

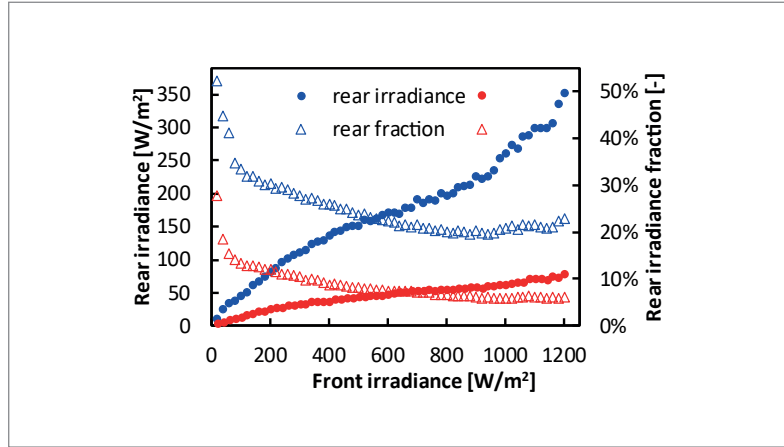


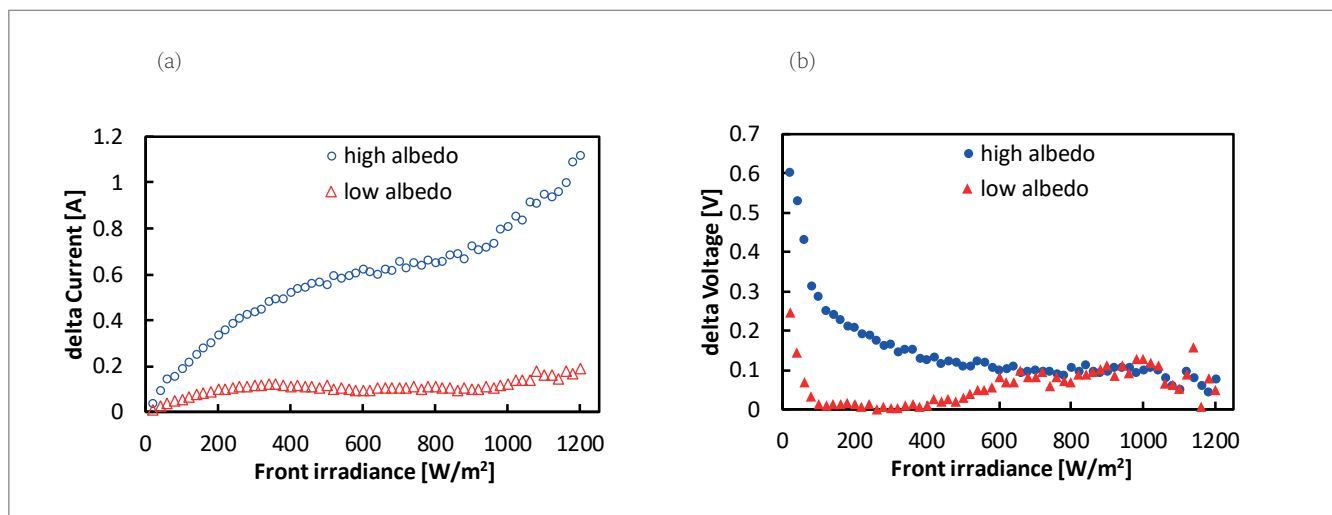
**Figure 7. Average rear irradiance and rear irradiance fraction as a function of the front irradiance.**

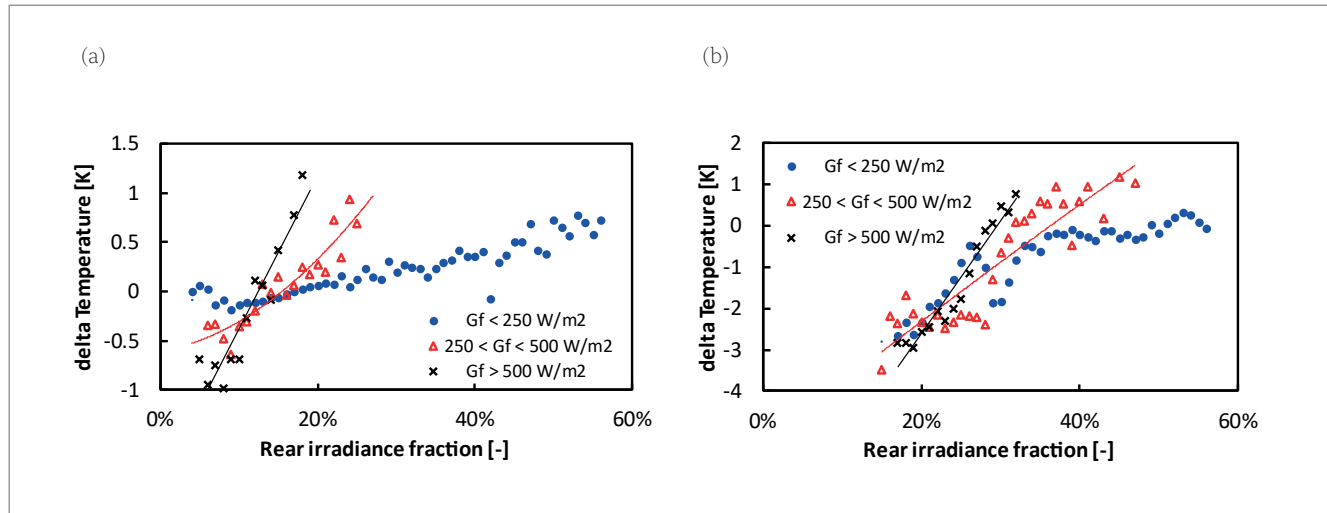
First, when the irradiance is dominated by diffuse irradiance, the front irradiance is low, but the diffuse irradiance is still incident on the rear side too, leading to a higher rear irradiance fraction than for clear-sky conditions. Second, because of the set-up and location, i.e. 30-degree tilt and latitude 51° N, in the summer months the rear sides of the panels are exposed to direct irradiance in the early and late hours of the day, leading to rear irradiance fractions in the range 50–90%.

Fig. 8(a) shows the difference in  $I_{\text{sc}}$  for the bifacial and monofacial modules; for all front-irradiance conditions,  $I_{\text{sc}}$  is larger for the bifacial module than for the monofacial one. The shape of the  $\Delta I_{\text{sc}}$  curves is very similar to that of the rear irradiance curves in Fig. 7 for the same albedo. Fig. 8(b) shows the difference in  $V_{\text{oc}}$ ; at a high front irradiance,  $G_t > 600\text{W/m}^2$ , the difference in  $V_{\text{oc}}$  for high and low albedos is very similar, around 0.1V, despite the much higher  $I_{\text{sc}}$  for the bifacial module under these conditions.

In low front-irradiance conditions, the difference between the values for low and high albedos is much larger. Whereas at low albedo the  $\Delta V_{\text{oc}}$  is around 0V between 100 and 400W/m<sup>2</sup>, at high albedo the  $\Delta V_{\text{oc}}$

**Figure 8. Average differences in (a)  $I_{\text{sc}}$  and (b)  $V_{\text{oc}}$  for the bifacial and monofacial modules, as a function of the front irradiance.**





**Figure 9. Average differences in module temperature as a function of the rear irradiance fraction for bifacial and monofacial modules: (a) low albedo; (b) high albedo. The data have been split into three groups: low irradiance  $<250\text{W/m}^2$ , intermediate irradiance, and high irradiance  $>500\text{W/m}^2$ . Lines have been drawn as visual references. (Note: a negative  $\Delta T$  means that the bifacial module is cooler than the monofacial module.)**

starts to increase. Below  $100\text{W/m}^2$  front irradiance, the average  $V_{oc}$  of the bifacial modules becomes much larger than that of the monofacial modules. This reflects the direct irradiance on the rear of the modules at the end of the day during the summer months, and that at low irradiance, the  $V_{oc}$  is more sensitive to additional irradiance. The bifacial  $V_{oc}$  is higher, despite the possibly higher module temperature under those low front-irradiance conditions.

Fig. 9 shows the average of the difference in module temperature between bifacial and monofacial modules for low and high albedo conditions as a function of the rear irradiance fraction. For both albedo conditions, the data have been divided into three front irradiance groups. At high albedo the minimum rear irradiance fraction is 16%, whereas at low albedo the minimum rear irradiance fraction is 4%. In addition, the range of the rear irradiance fraction is smaller for the high front irradiance group ( $>500\text{W/m}^2$ ) than for the low front irradiance group ( $<250\text{W/m}^2$ ).

The two graphs in Fig. 9 show the same behaviour: 1) with increasing rear irradiance fraction, the  $\Delta T$  increases; 2) the slope of this trend increases with increasing front irradiance group; 3) at low rear irradiance fraction, the bifacial module is cooler, by 1 to 3K, than the monofacial module; and 4) at high rear irradiance fraction, the bifacial module is warmer, by up to 1K, than the monofacial module. It is important to realize that in the conditions that lead to warmer bifacial modules, i.e. rear irradiance fraction  $>30\%$ , the increase in voltage and current will yield a much larger increase in output power

than the  $\sim 0.5\%$  decrease in power due to the increased module temperature.

These findings corroborate what had been deduced from the lab experiments. Fig. 4 showed that with increasing rear irradiance, the effective heat input for the bifacial module type increases faster than for the WBS module architecture. Thus, with increasing rear fraction, the bifacial heat input increases faster, leading to a larger increase in bifacial module temperature. Consequently, with increasing rear irradiance fraction, there is a shift from cooler bifacial modules at low rear irradiance (fraction) to warmer bifacial modules at high rear irradiance (fraction).

To summarize, at high rear irradiance fractions, bifacial modules can be warmer; how much depends on the irradiance level as well. The total decrease in energy yield, however, will be small, and if this occurs at a high albedo, the resulting additional yield gain will still be significant.

## Conclusions

Background theory and indoor and outdoor measurements have been presented in order to provide a better understanding of the differences in thermal behaviour between monofacial and bifacial modules.

The effective heat input  $Q_{\text{eff}}$  for monofacial and bifacial solar cells and modules is derived from energy spectra on the basis of indoor measurements. This information is used as input for the module characteristics in ECNTNO's bifacial energy yield model BIGEYE [12]. Although  $Q_{\text{eff}}$  increases faster with rear irradiance for glass–glass samples than for monofacial modules, under outdoor conditions the increase in device temperature is identical for Al-BSF cells, irrespective of rear panel material. For n-PERT solar cells in glass–glass mini-modules, a lower temperature than that for monofacial n-PERT devices is even found. This can be explained by the glass–glass modules having a higher heat transfer

**“Even in cases where high rear irradiance leads to warmer bifacial modules, the energy gain due to the bifaciality is much higher than the eventual losses due to slight heating.”**

coefficient  $U$ , just as was found from indoor heating curves under constant irradiance. Clearly, the higher  $U$  compensates for the higher  $Q_{\text{eff}}$ .

On ECNTNO's rooftop installation, it was shown that at high rear irradiance fractions, bifacial 60-cell modules can be warmer; how much warmer depends on the irradiance level as well. The total contribution to the yield, however, will be small, as these conditions typically occur at low total irradiance, although at high albedo the additional power is still significant. Under high front-irradiance conditions, when the rear irradiance fraction is low the bifacial module is cooler, despite the rear irradiance photocurrent generation.

To conclude, even in cases where high rear irradiance leads to warmer bifacial modules, the energy gain due to the bifaciality is much higher than the eventual losses due to slight heating. Changes in the bill of materials, e.g. to account for thinner glass, could shift the cross-over point by increasing the effective heat transfer  $U$ , and thus decrease the steady-state temperature of the bifacial PV panels relative to monofacial ones, even under high albedo conditions.

## References

- [1] Olukan, T.A. & Emziane, M. 2014, "A comparative analysis of PV module temperature models", *Energy Procedia*, Vol. 62, pp. 694–703.
- [2] Dekker, N.J.J. et al. 2015, "Accurate yearly yield calculation using PV module fingerprint method – Applied for MWT, H-pattern and thin film module", *Proc. 31st EU PVSEC*, Hamburg, Germany, pp. 2047–2050.
- [3] Hansen, C. et al. 2017, "A detailed performance model for bifacial PV modules", *Proc. 33rd EU PVSEC*, Amsterdam, The Netherlands, pp. 2395–2400.
- [4] SolarWorld 2015, "Calculating the additional energy yield of bifacial solar modules", White Paper [<https://www.solarworld-usa.com/~media/www/files/white-papers/calculating-additional-energy-yield-through-bifacial-solar-technology-sw9002us.pdf?la=en>].
- [5] Soria, B. et al. 2016, "A study of the annual performance of bifacial photovoltaic modules in the case of vertical facade integration", *Energy Sci. Eng.*, Vol. 4, No. 1, pp. 52–68.
- [6] Lopez-Garcia, J., Pavanello, D. & Sample, T. 2018, "Analysis of temperature coefficients of bifacial crystalline silicon PV modules", *IEEE J. Photovolt.*, Vol. 8, No. 4, pp. 960–968.
- [7] Tiedje, T., Yablonovitch, E.D.C.G. & Brooks, B.G. 1984, "Limiting efficiency of silicon solar cells", *IEEE Trans. Electron Dev.*, Vol. 31, pp. 711–716.
- [8] Baker-Finch, S.C. et al. 2014, "Near-infrared free carrier absorption in heavily doped silicon", *J. Appl. Phys.*, Vol. 116, No. 6, 063106.
- [9] Clugston, D.A. & Basore, P.A. 1997, "Modelling free-carrier absorption in solar cells", *Prog. Photovolt. Res. Appl.*, Vol. 5, pp. 229–239.
- [10] Vogt, M.R. et al. 2015, "Numerical modeling of c-Si PV modules by coupling the semiconductor with the thermal conduction, convection and radiation equations", *Energy Procedia*, Vol. 77, pp. 215–224.
- [11] Romijn, I.G. et al. 2012, "Industrial implementation of efficiency improvements in n-type solar cells and modules", *Proc. 27th EU PVSEC*, Frankfurt, Germany, pp. 533–537.
- [12] Janssen, G.J.M. et al. 2018, "How to maximize the kWh/kWp ratio: Simulations of single-axis tracking in bifacial systems", *Proc. 35th EU PVSEC*, Brussels, Belgium, pp. 1573–1577.
- [13] Roest, S. et al. 2017, "Single side versus double side illumination method IV measurements for several types of bifacial PV modules", *Proc. 33rd EU PVSEC*, Amsterdam, The Netherlands, pp. 1427–1431.
- [14] Hoang, P. et al. 2014, "Coupling optical and thermal models to accurately predict PV panel electricity production", *Sol. Energy Mater. Sol. Cells*, Vol. 125, pp. 325–338.
- [15] Van Aken, B.B. & Carr, A.J. 2014, "Relating indoor and outdoor performance of bifacial modules", *Proc. 40th IEEE PVSC*, Denver, Colorado, USA, pp. 1381–1383.

## About the Authors

Dr. Bas Van Aken is a specialist scientist on the systems, modules and applications team in the solar energy research group at ECNTNO, focusing on fabrication, reliability and (outdoor) performance of bifacial and back-contact modules. He previously worked on thin-film Si solar cells processed by PECVD. After gaining a Ph.D. in solid state chemistry at the University of Groningen in the Netherlands, he worked as a postdoc at Cambridge University and at the Max Born Institute for Nonlinear and Ultrafast Optics in Berlin.

Dr. Gaby Janssen received a Ph.D. in quantum chemistry from the University of Groningen. After joining ECN, she worked as a research scientist on the simulation, characterization and optimization of materials for energy conversion technologies, in particular fuel cells. In 2011 she joined the solar energy department, now a research group, at ECNTNO, where she focuses on simulation and modelling of PV cells and modules. Over the last few years she has developed an energy yield prediction model for bifacial systems.

## Enquiries

ECNTNO – Solar Energy  
PO Box 15  
1755 ZG Petten  
The Netherlands

Email: [basvanaken@tno.nl](mailto:basvanaken@tno.nl)